

宇宙学漫谈：从星空到暗能量

傅慎明

杭高天文社20周年纪念讲座

2023年1月28日

自我简介

- 杭高 2008-2011
- 中科大 2011-2015
- 布朗大学 2015-2021
- NOIRLab 2021-now
- 研究方向：星系团引力透镜，时域天文，
测光红移，星系团宇宙学



提纲

1. 星空与很久以前的天文神话，不同文明的交流
2. 从400年前望远镜的发明说开去
3. 100年前人们发现宇宙膨胀
4. 近几十年的观测让人们如何理解宇宙；暗物质，暗能量，引力波

第一部分

从看星星说起

- 星空很美
- 不过，让我们来想一想，星空告诉了我们什么信息呢
- 假如我们仔细观察：（为什么会有这些现象）
 - 星星会闪烁，不同星星闪烁的幅度不一样
 - 星星有不同颜色
 - 观察一段时间，我们发现星星会动，而且有周期性
 - ...

周期性

- 让我们想象几千年以前古人的生活
- 对于古人来说，周期性非常重要——可以用来计时——用于生产生活，例如农耕狩猎
- 我们的生活体验：人对时间的感知是弱于对空间的感知的
- 有周期性的事物成了很好的计时工具：日月星辰
- 周期性也意味着确定性

古人如何理解星空

- 古人没有现代天文学知识，但他们看到的天空和我们看到的相似
- 他们总结出什么规律？
- 他们怎么理解这些现象和规律？

“帝尧者，放勋。…乃命羲、和，敬顺昊天，数法日月星辰，敬授民时。…日中，星鸟，以殷中春。…日永，星火，以正中夏。…夜中，星虚，以正中秋。…日短，星昴，以正中冬。…岁三百六十六日，以闰月正四时。”

《史记·五帝本纪》

中：平分。鸟：朱雀（双子、巨蟹、狮子、长蛇等）。火：大火（心宿二）。虚宿：宝瓶、小马，靠近飞马、海豚。

天体与时间

- 与时间有关的文字: 日 (dial) , 月 (moon/month) , 黄道十二宫 (zodiac/zoo)
- 岁星, 镇星
- 星期: Monday/Lunes (Moon), Tuesday/Martes (Tiw/Mars), Wednesday/Miércoles (Odin/Mercury), Thursday/Jueves (Thor/Jupiter), Friday/Viernes (Frigga/Venus), Saturday/Sábado (Saturn), Sunday/Domingo (Sun)
- ...

天文神话

- 中外有很多大家熟知的神话故事
- 天文神话故事代表了古人对宇宙的朴素理解，成为社会生活的重要媒介
- 神话故事尝试回答这些问题：
 - 时间，空间，以及中间的事物从何而来？
 - 什么决定了天体的运动？
 - 如果说那是由一种神秘的力量导致的，那么那种力量是否也影响着地面上的事物，尤其是人的命运？

第二部分

- 快进到400年前，逐渐祛魅
- 大自然不再神秘——天上和地上的事物（大自然 vs 现实生活），慢慢失去了人们以为的“联系”



望远镜 1

- 伽利略：木星卫星（1610; 马里乌斯），不光滑的月球，“三颗星”的土星
- 宇宙的中心在哪里？
- 牛顿：万有引力，解释开普勒定律。哈雷：彗星（1759）
- 爱因斯坦等：相对性原理。物理定律形式不变，与时间无关，与地点无关，与参考系无关，只有坐标变换

一些引申的问题

- 归纳法一定有效吗？或者是一种概率？
- 是否存在绝对正确的物理定律？还是仅仅是模型（在一定条件下适用）？
- 物理定律的自洽性，简洁性（奥卡姆剃刀）

第三部分

- 快进到一百年前，进入现代



宇宙膨胀：观测

- 沙普利：球状星团距离很远，银河系很大，太阳不是银河系的中心
- 哈勃，勒梅特 Lemaître： $v = c \times z = H_0 \times D$
- 宇宙学红移
- 宇宙比银河系大（“星系”在银河系之外）
- 宇宙在膨胀：银河系也不是宇宙中心
- 造父变星：周光关系（勒维特 Leavitt），距离测量

宇宙膨胀：理论

- 广义相对论：物质和时空的关系
- 均匀宇宙，FLRW度规
- 低红移与哈勃常数，高红移的距离
- $H_0 = H(t_0)$, $H = da/dt / a$
- H_0 tension

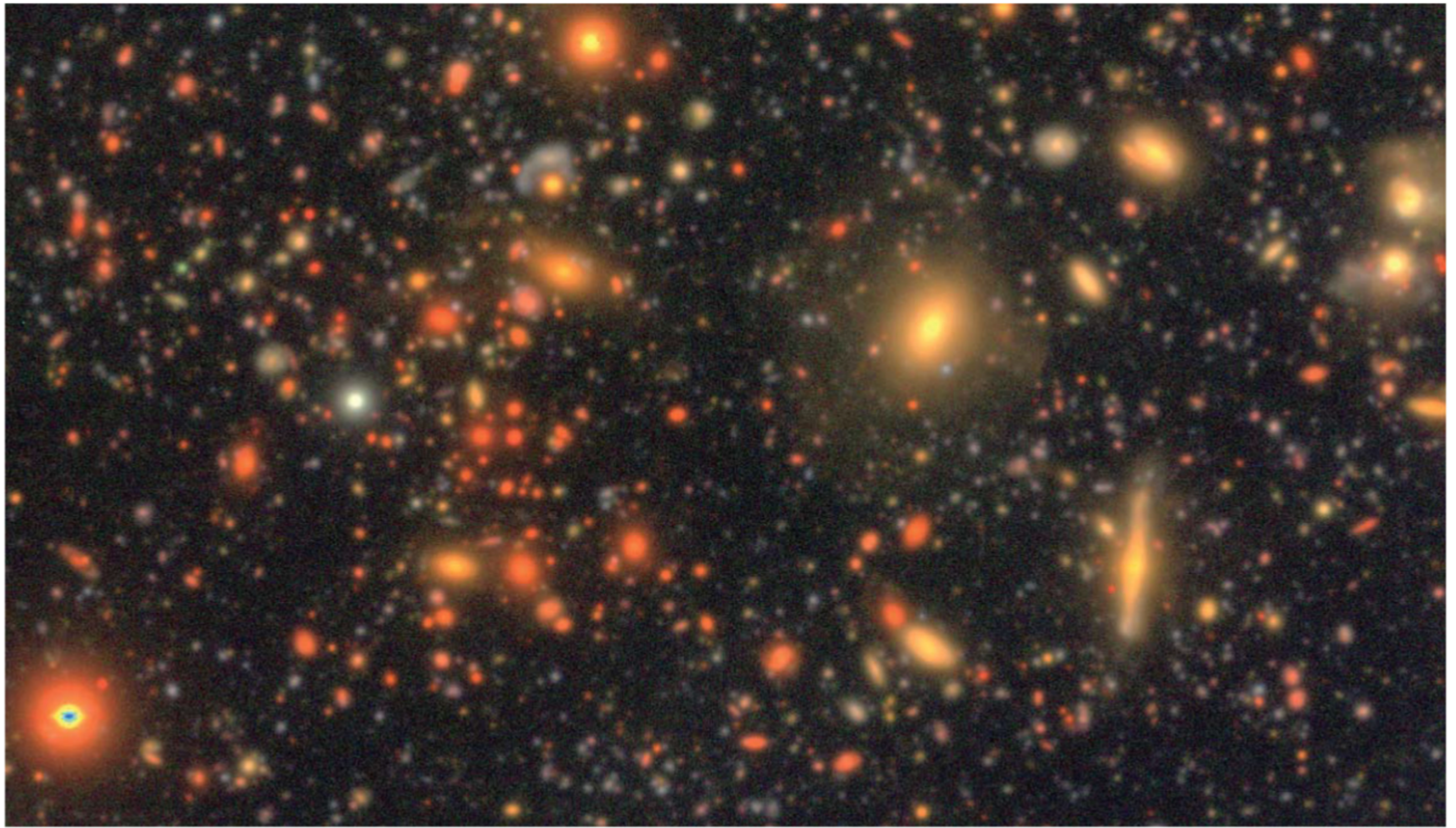
第四部分

- 几十年前到现在



望远镜 2

- 大型巡天望远镜
- 当我们看得足够深，放得足够大，能看到什么？
- 从大量的星星（银河系），到大量的星系（~22等）
- 其中的统计关系



HSC SSP PDR2 Aihara+2019 超深场 ~28等

Fig. 17. *gri* color-composite of a small chunk (3.5×2.0) of the COSMOS field centered at RA = $10^{\text{h}}00^{\text{m}}20^{\text{s}}.0$, Dec = $+02^{\circ}11'55''$. North is up. This image is colored following the algorithm of Lupton et al. (2004). (Color online)

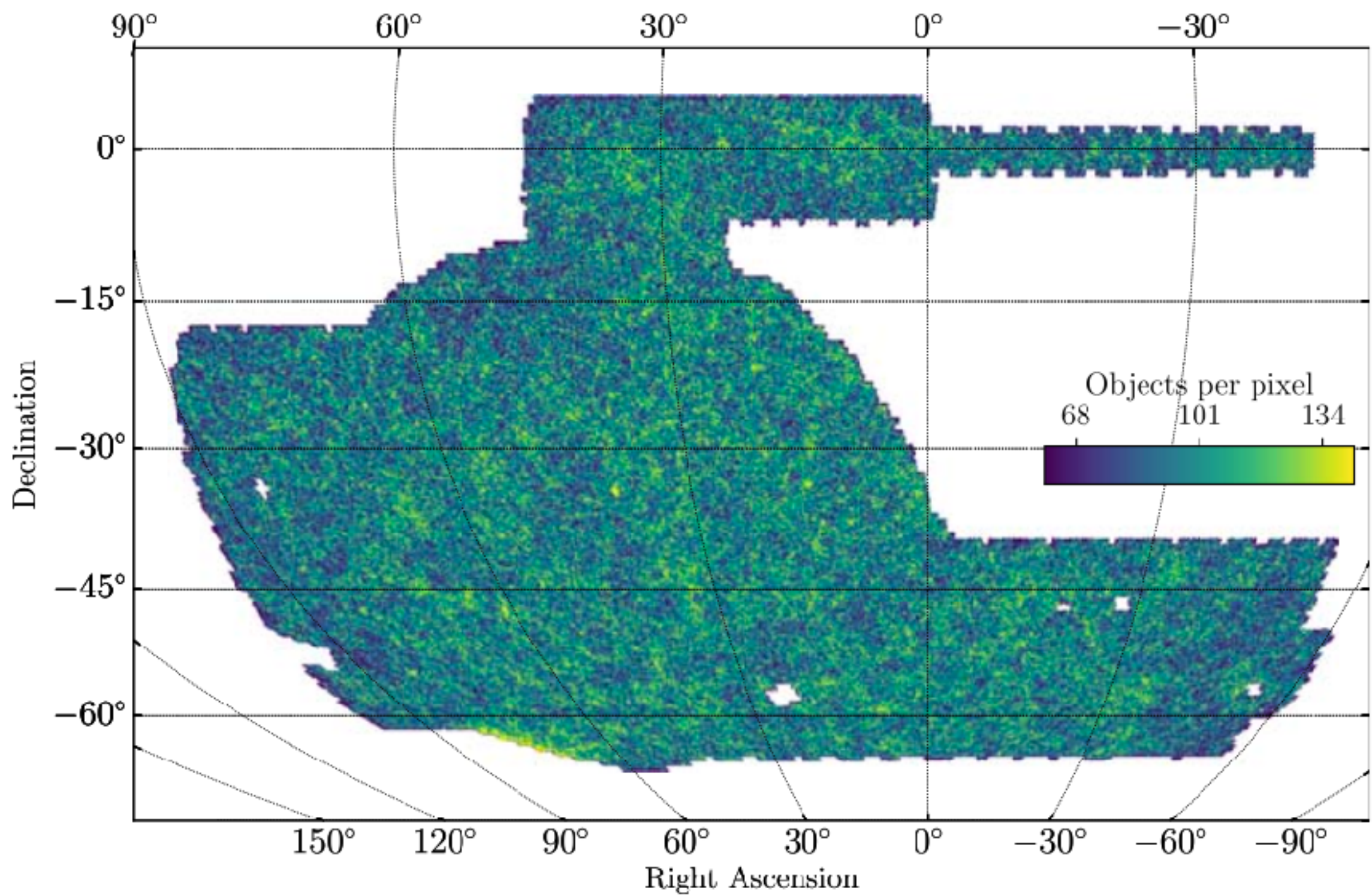
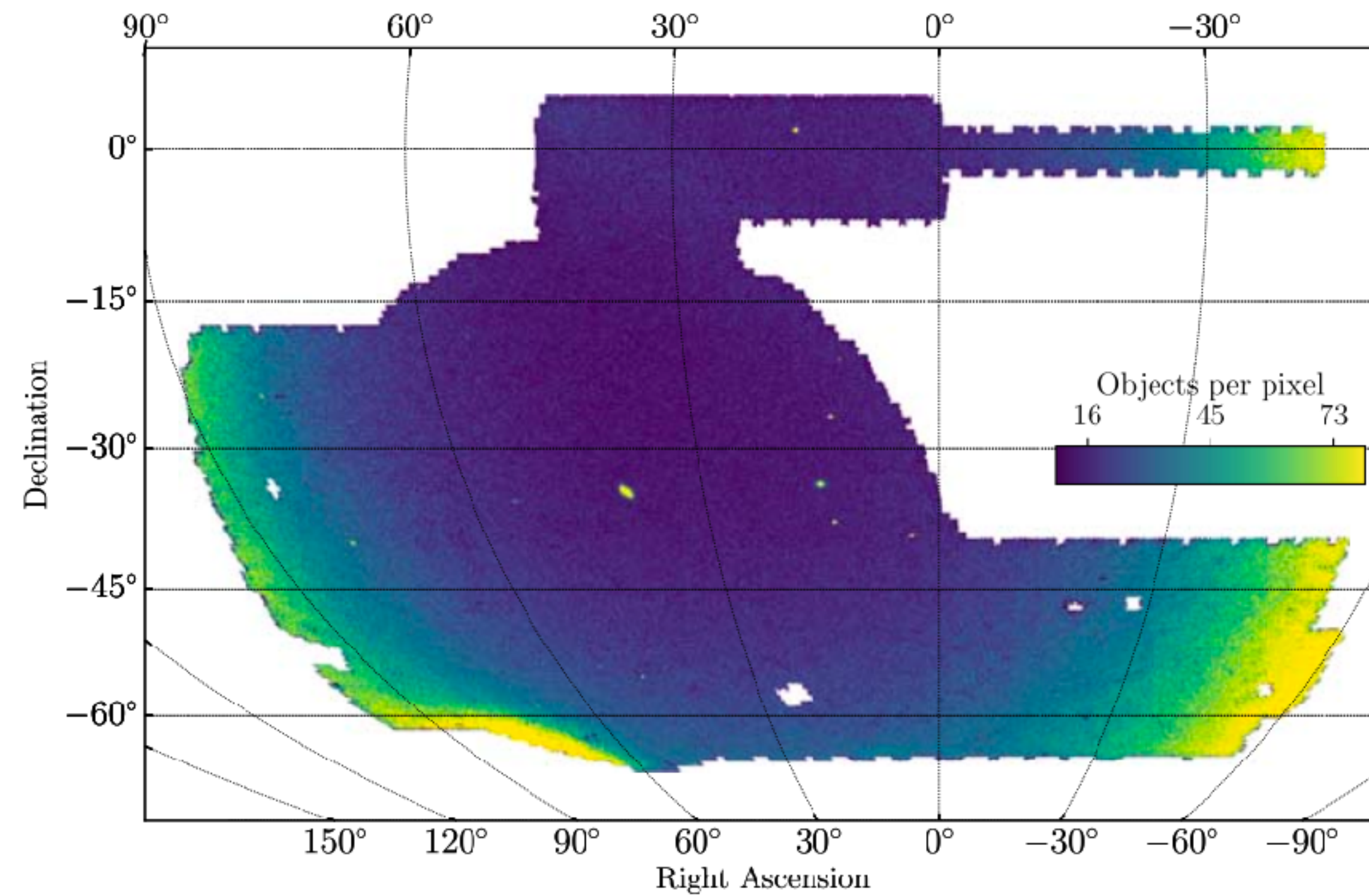
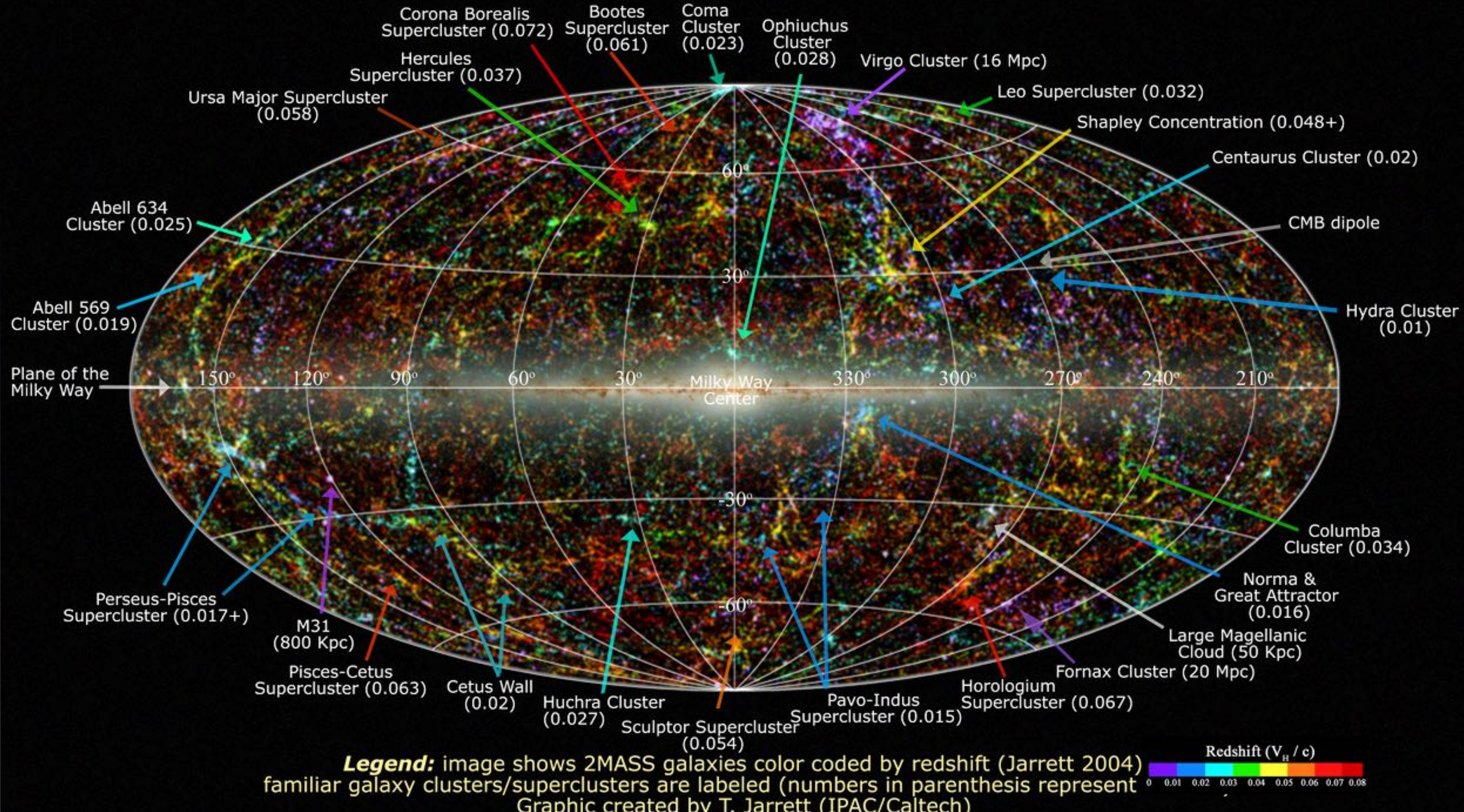


Figure 13. Left: map of stellar number counts created with the `EXTENDED_COADD = 0` selection described in Section 4.7. Discrete peaks in the stellar number counts correspond to globular clusters and dwarf galaxies in the Milky Way halo. Right: analogous galaxy number counts map created with the `EXTENDED_COADD = 3` selection. Color range units are the number of objects per HEALPix `nside = 1024` pixel without correcting for the coverage fraction of each pixel. Both maps use a magnitude threshold of `MAG_AUTO_I < 23`.

DES DR2 Abbott+2021 ~23等

Large Scale Structure in the Local Universe



仅含引力的多体模拟
Heitmann+2021
从大尺度下的均匀到
小尺度下的不均匀

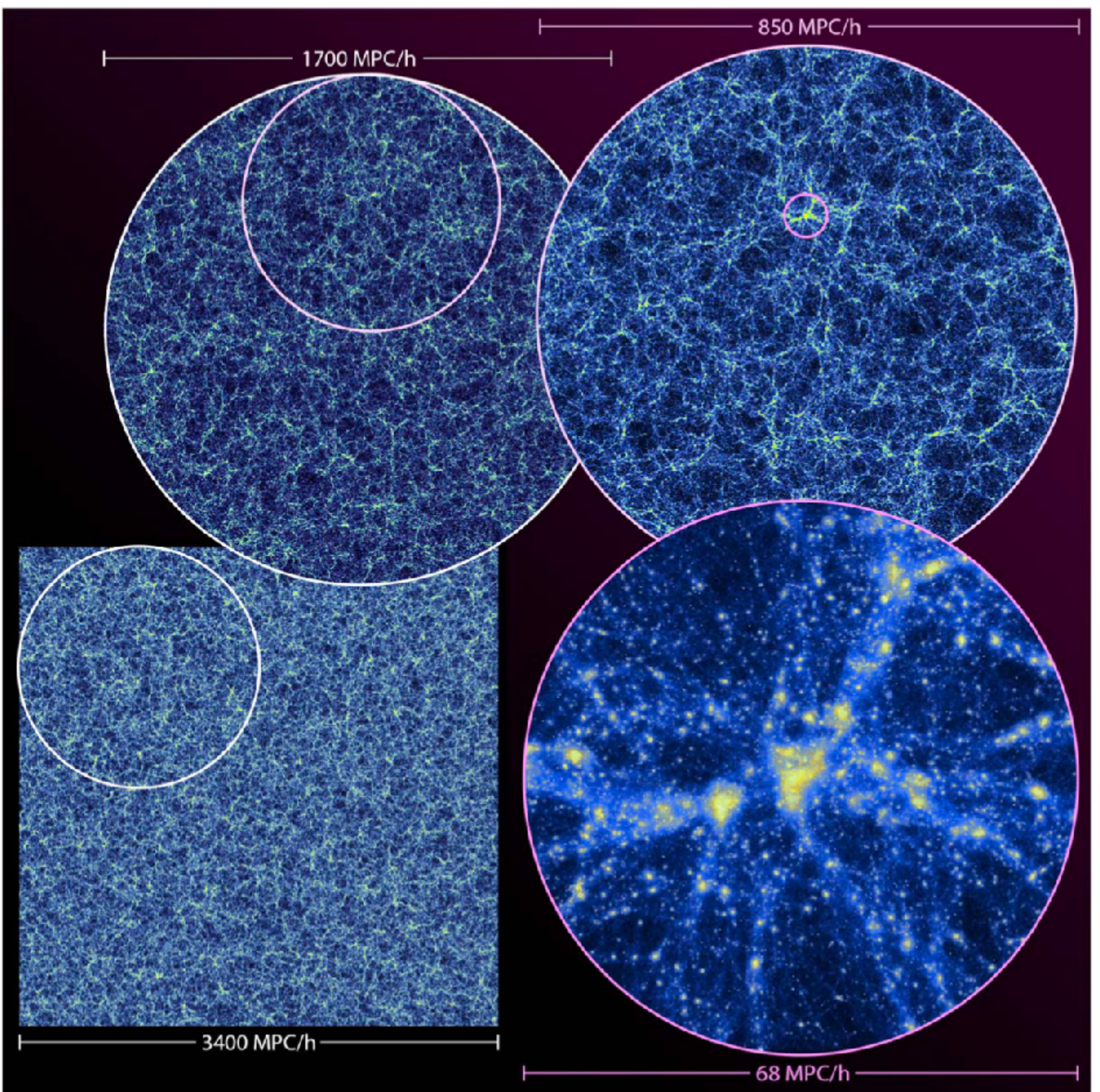


Figure 1. Visualization of the Last Journey simulation. Shown are thin density slices for the full box (lower left corner) and zoom-ins at different levels. The panel in the lower right corner focuses on the largest cluster in the simulation with a mass of $\sim 6 \cdot 10^{15} h^{-1} M_{\odot}$.

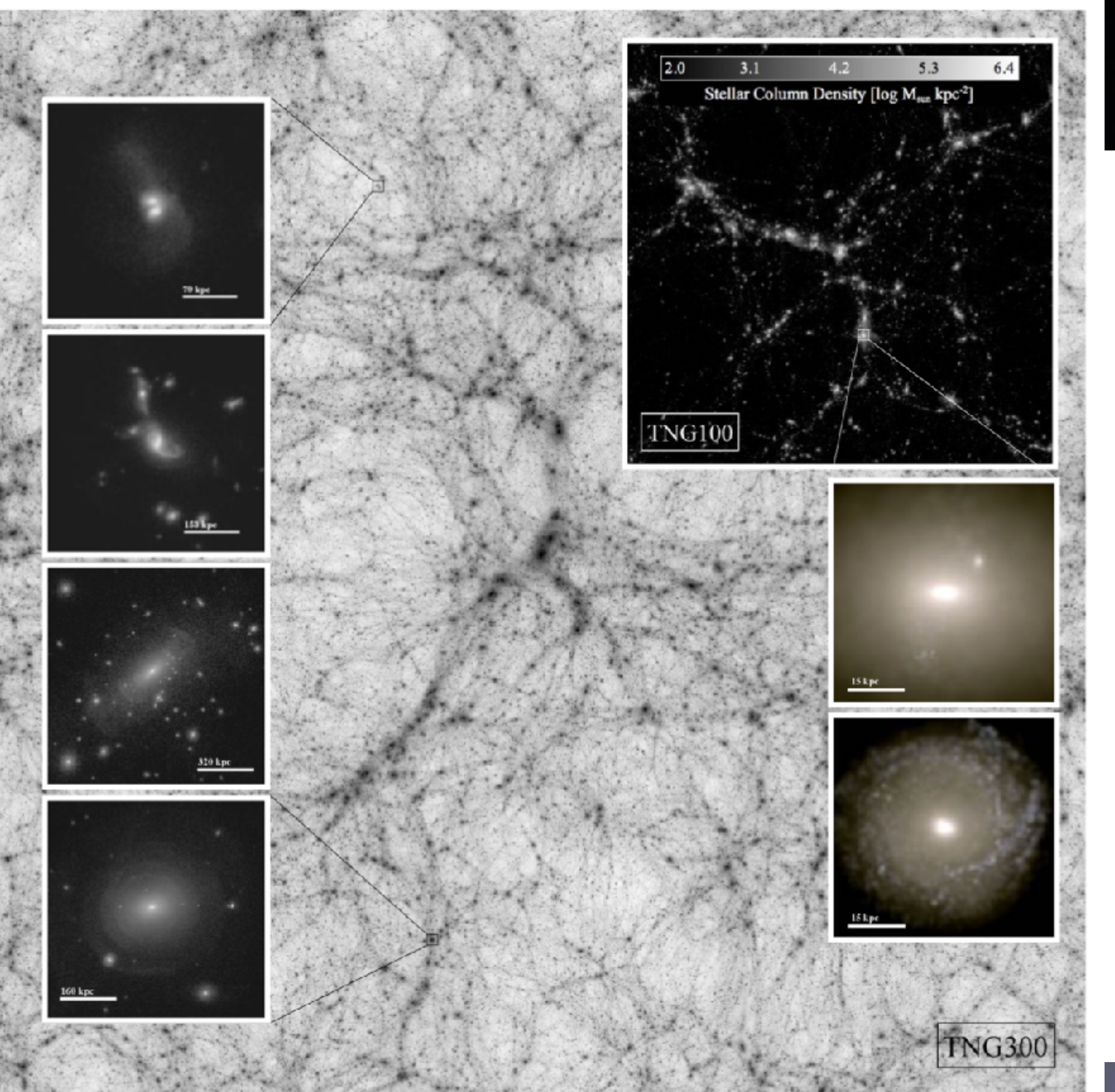


Figure 1. The IllustrisTNG simulations: $z = 0$ visual representation of the scope and spatial volumes encompassed by the TNG100 and TNG300 runs presented in this paper. The background represents the DM density field across the ~ 300 Mpc volume of TNG300, while the upper right inset shows the distribution of stellar mass across the entire ~ 100 Mpc volume of TNG100, each projected through a slice a third of the box in depth. Panels on the left show two examples of galaxy-galaxy interactions, and two examples of fine-grained structure of the extended stellar haloes – shells, tidal tails, and luminous satellites – around two massive ellipticals at $z = 0$, in projected stellar mass density. The bottom right insets show the stellar light on scales of 60 kpc per side (face-on) of two randomly selected $z = 0$ galaxies with a stellar mass larger than $10^{11} M_{\odot}$, from the high-resolution TNG100 box.

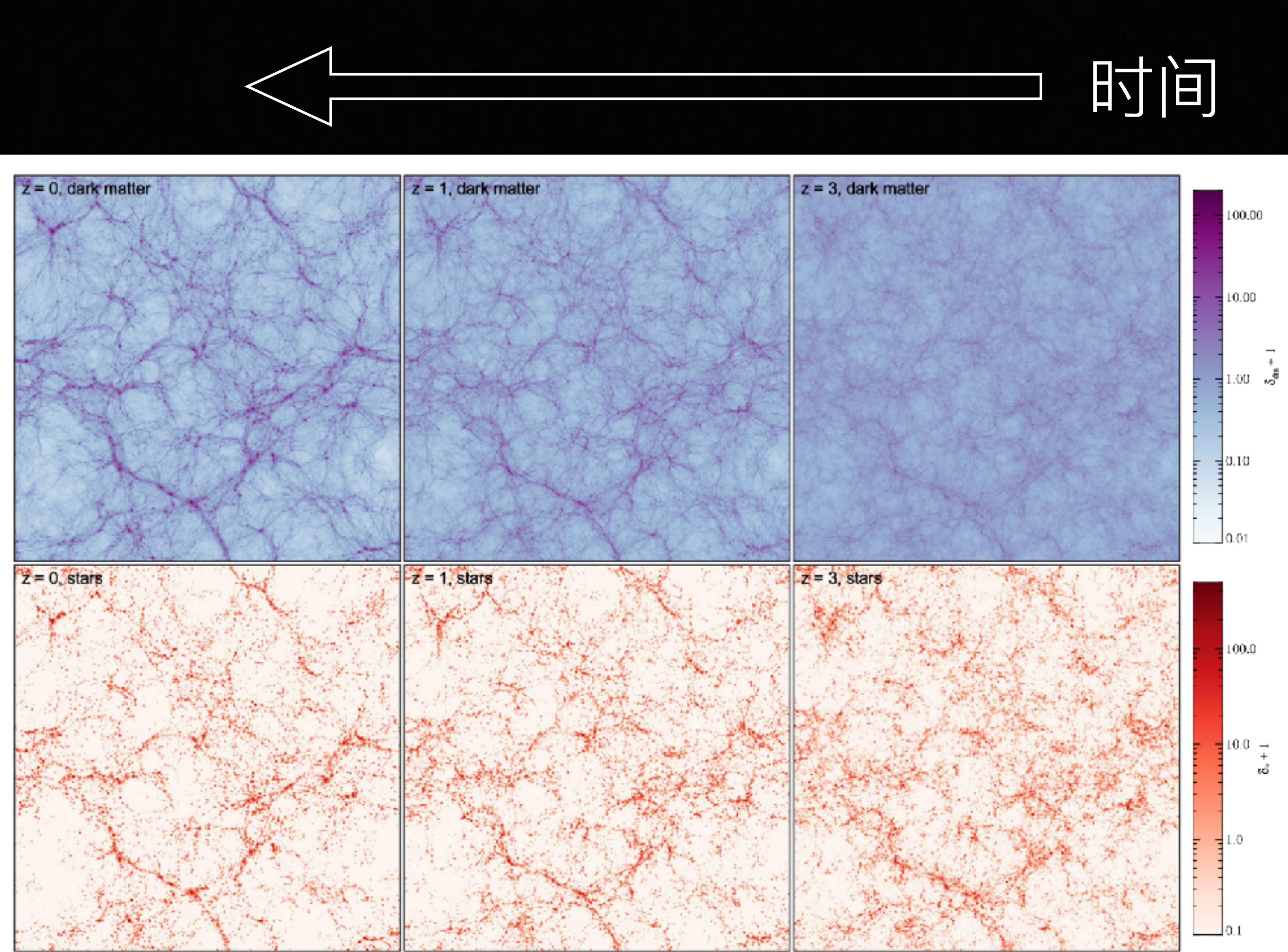


Figure 2. Projected DM and stellar density fields in TNG300, at redshifts $z = 0, 1$, and 3 . The slices are $205 h^{-1}$ Mpc wide (full width of the box) and $25 h^{-1}$ Mpc thick, with the density fields being normalized to the mean density in each panel. The density field of the stars has been smoothed with a Gaussian filter of width $160 h^{-1}$ kpc to make it more volume filling and hence better visible. While the density contrast in the DM distribution progressively increases with time, the clustering of the stellar matter is already strong at high redshift and evolves little with time.

暗物质+磁流体模拟：星系形成；边长 ~ 300 Mpc
Pillepich+2018; Springel+2018

宇宙学原理

- 均匀各向同性 (大尺度/早期宇宙)
- 奥伯斯佯谬 → 时间是有限的，红移

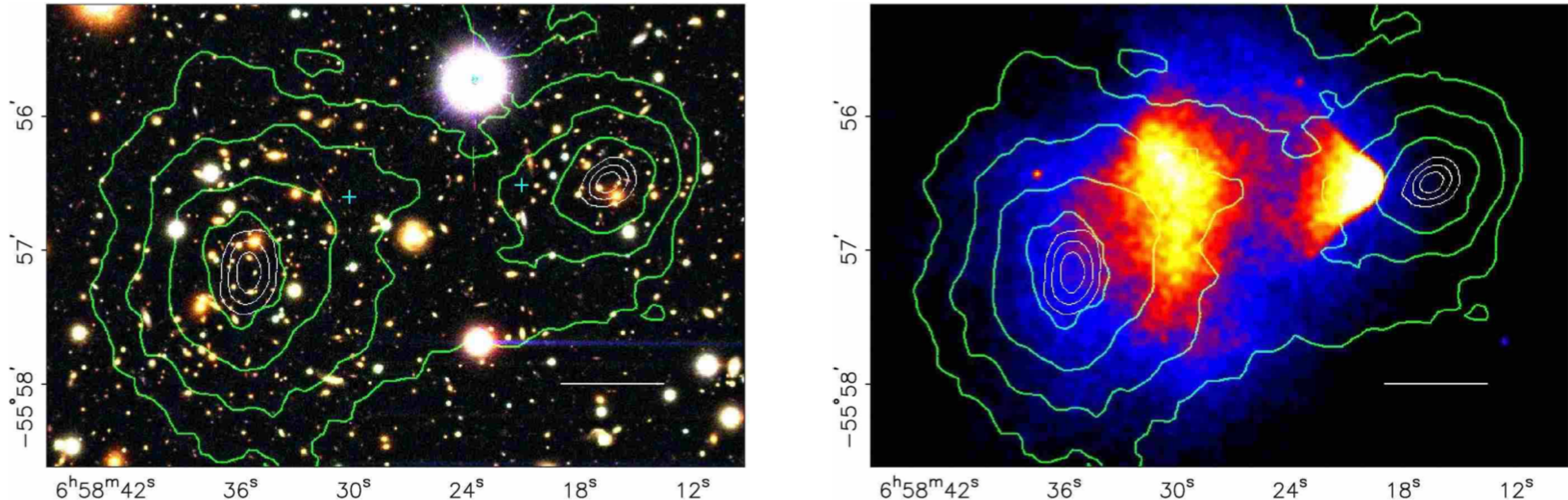
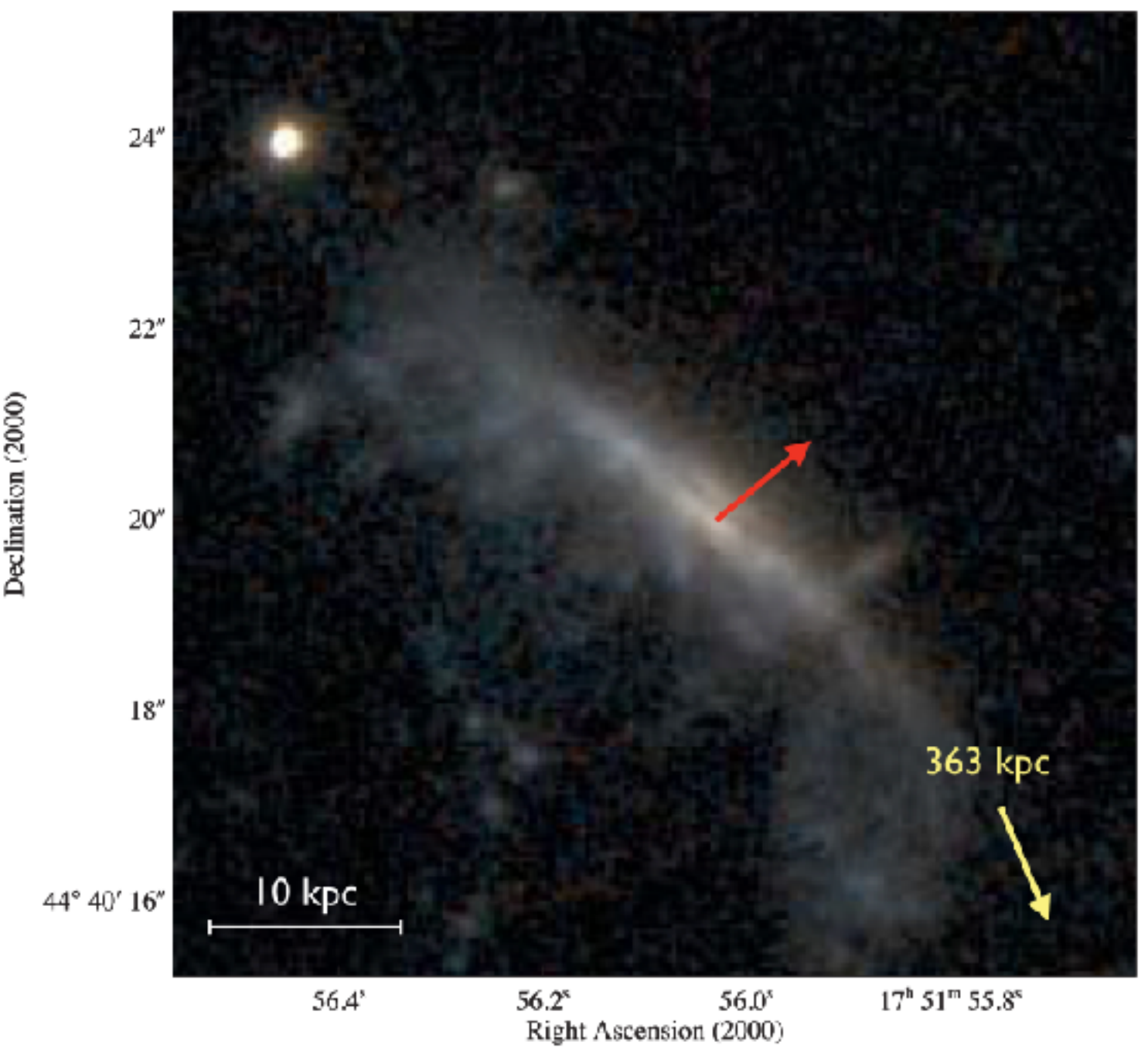
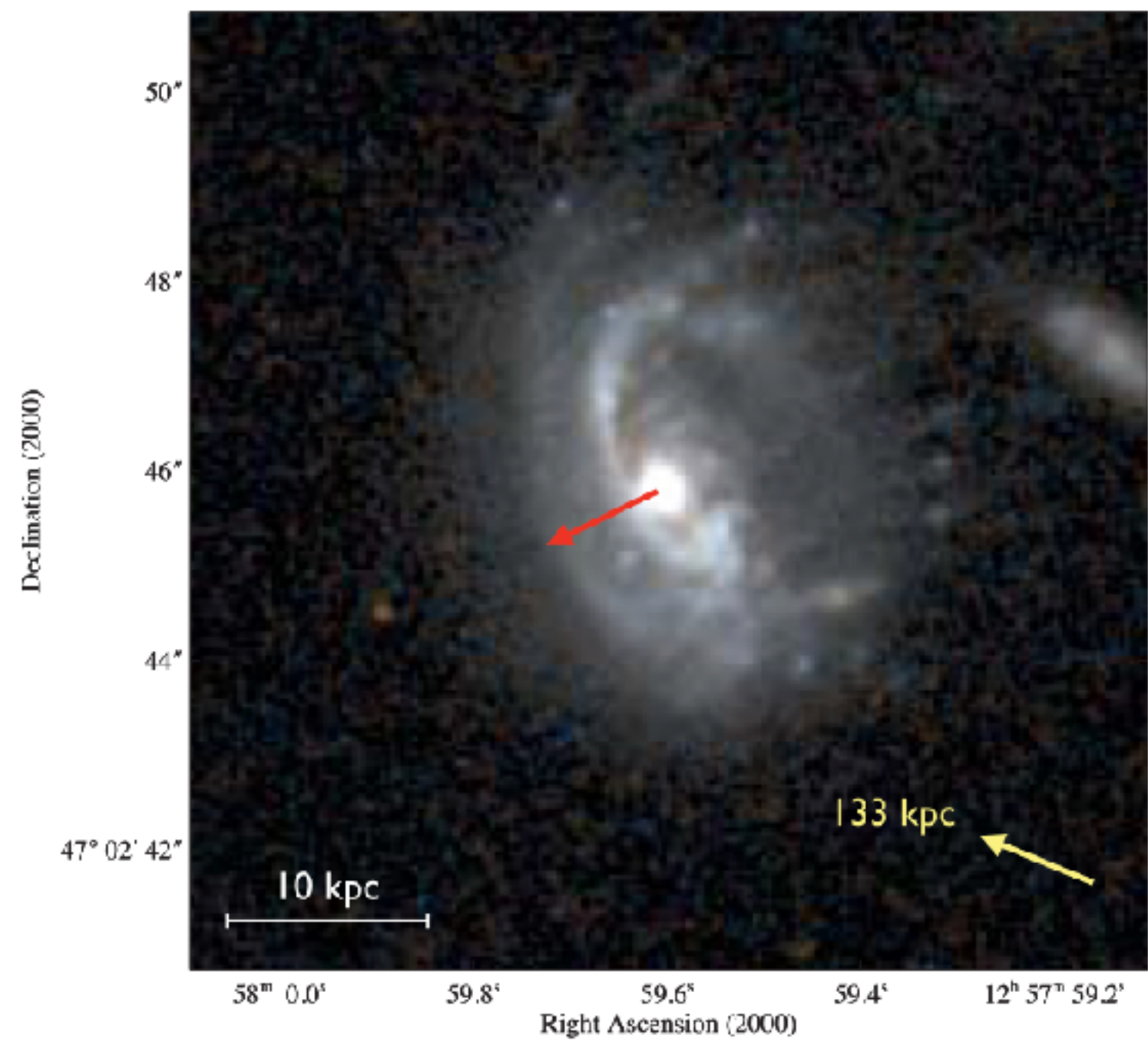
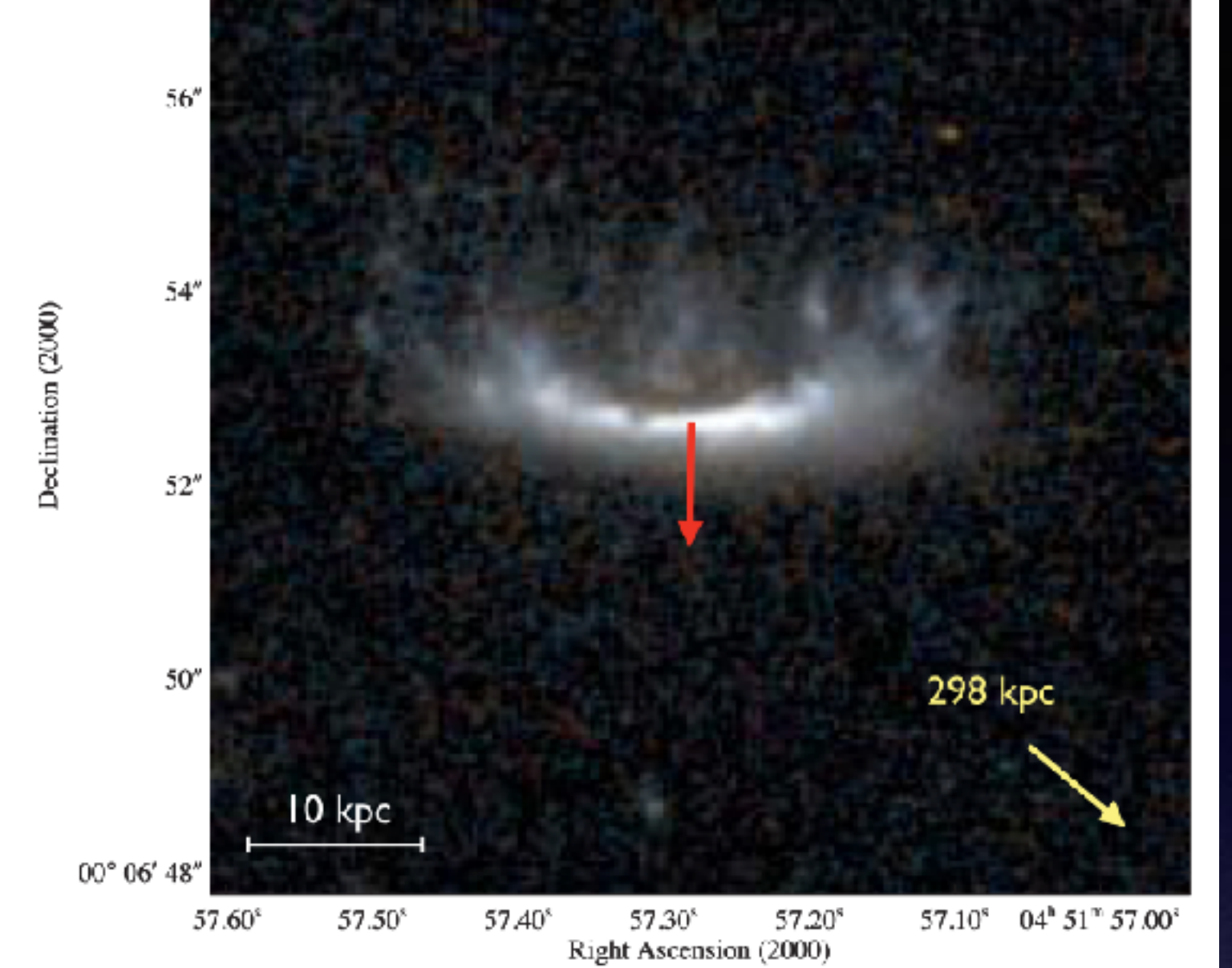
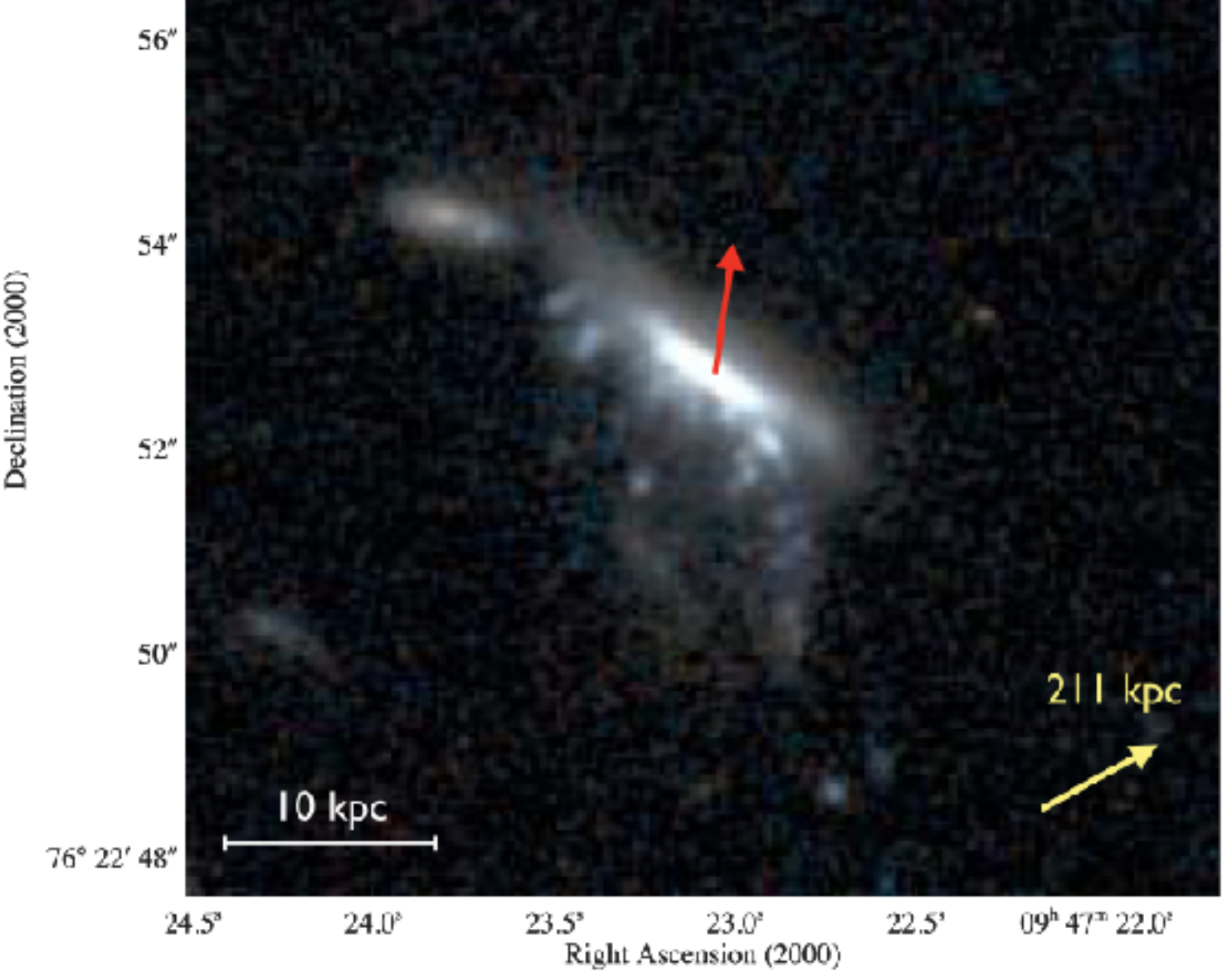
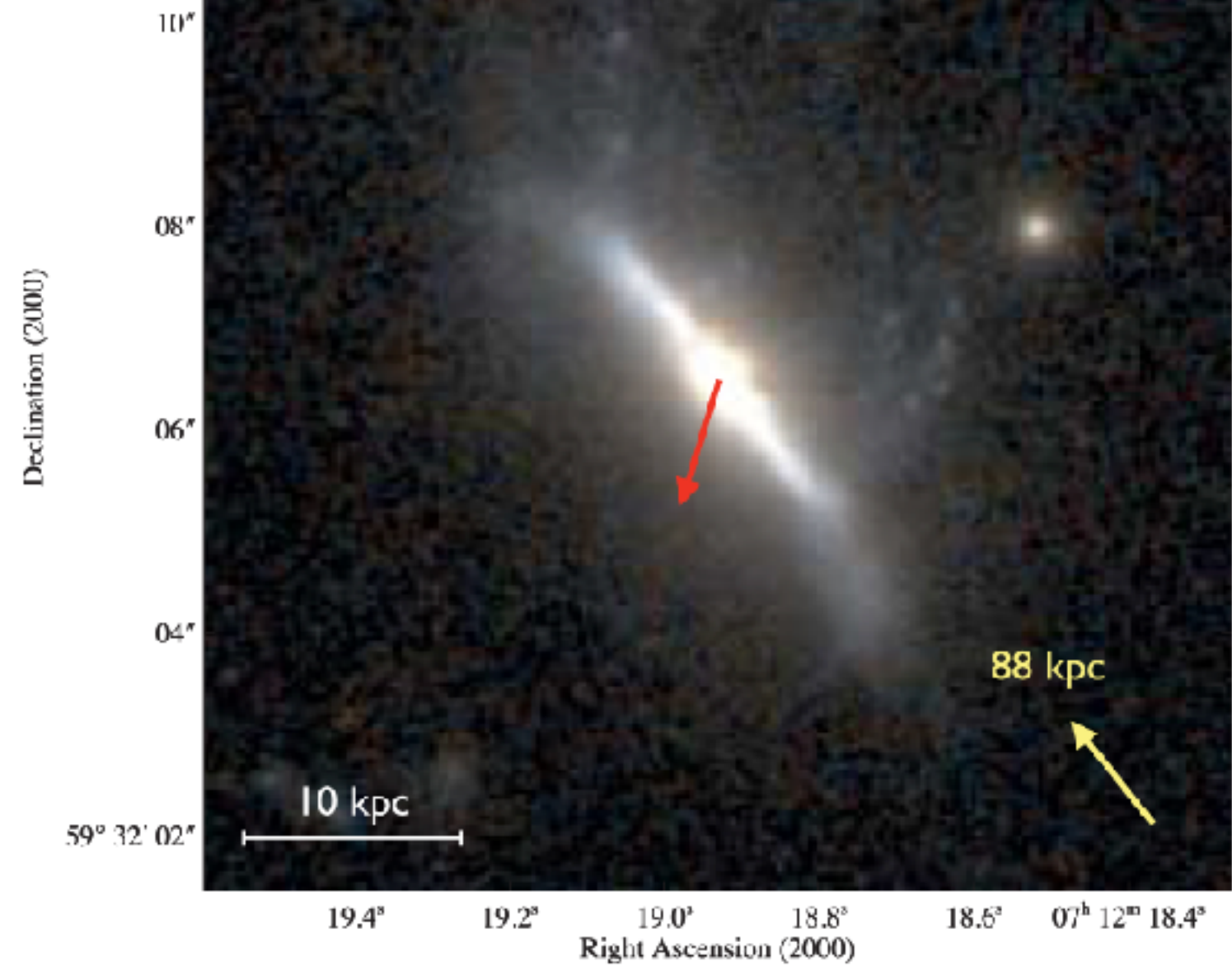


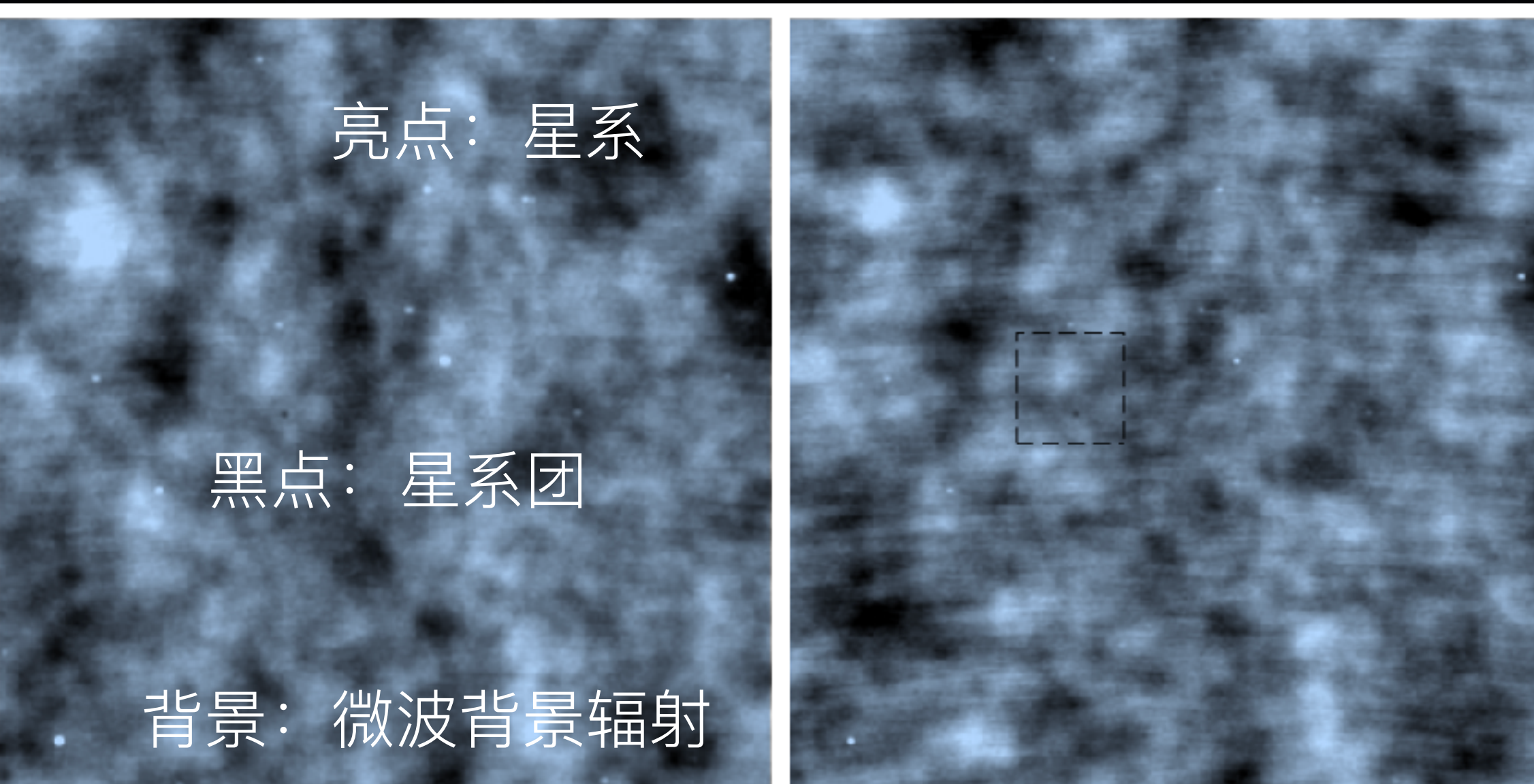
FIG. 1.— Shown above in the top panel is a color image from the Magellan images of the merging cluster 1E0657–558, with the white bar indicating 200 kpc at the distance of the cluster. In the bottom panel is a 500 ks Chandra image of the cluster. Shown in green contours in both panels are the weak lensing κ reconstruction with the outer contour level at $\kappa = 0.16$ and increasing in steps of 0.07. The white contours show the errors on the positions of the κ peaks and correspond to 68.3%, 95.5%, and 99.7% confidence levels. The blue +s show the location of the centers used to measure the masses of the plasma clouds in Table 2.

“子弹”星系团
Clowe+2006



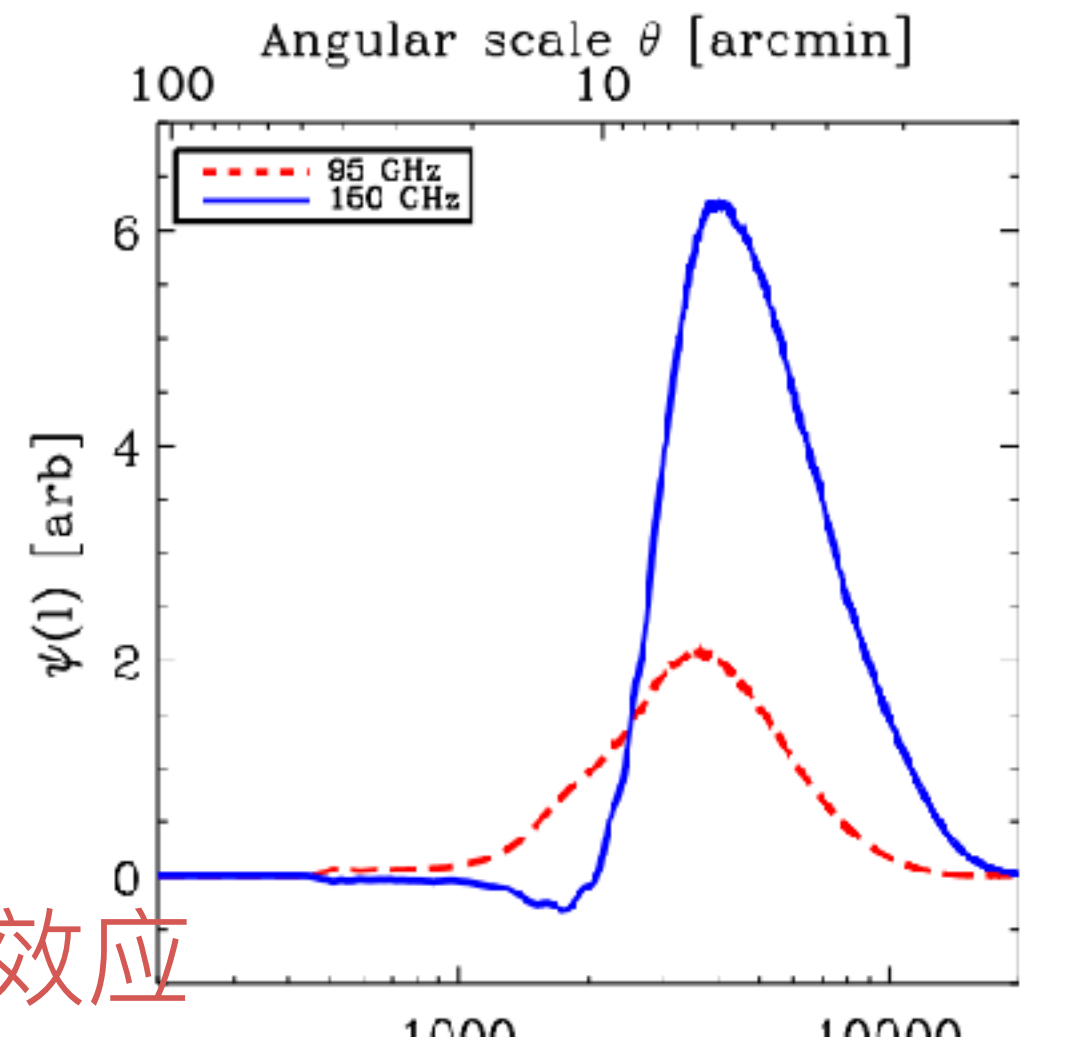
“水母”星系
Ebeling+2014

Figure 2. HST images (F606W+F814W) of extreme cases of ram-pressure stripping in MACS galaxy clusters at $0.30 < z < 0.43$. In each panel, the direction and projected distance to the cluster center (as given by the location of the BCG) is marked in the bottom right corner; red arrows denote the approximate direction of motion of the respective galaxy.



(a) 95 GHz minimally filtered map cutout

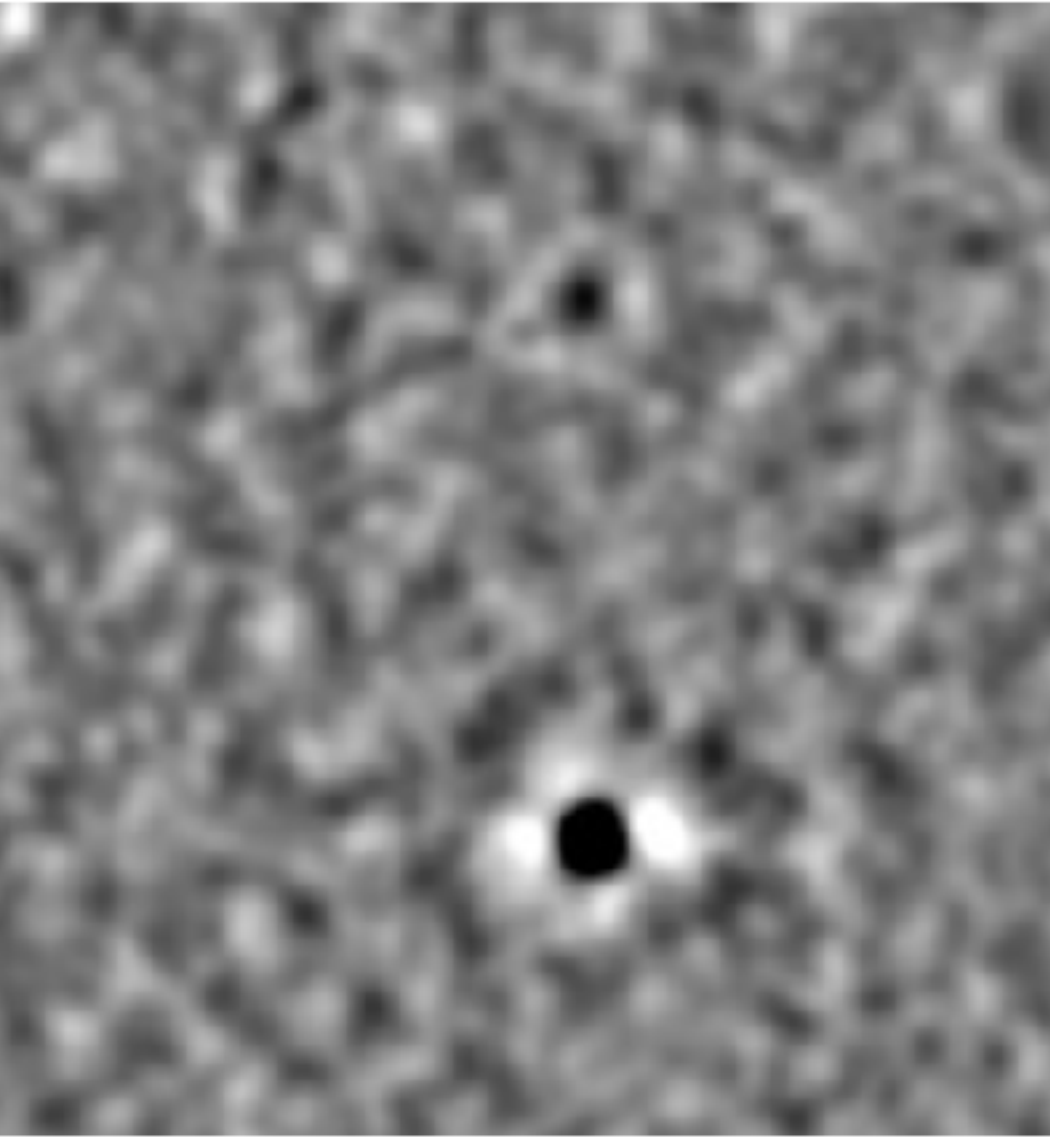
(b) 150 GHz minimally filtered map cutout



SZ效应

Bleem+2015

(c) Azimuthally averaged cluster-matched two-band filter



(d) Cluster-filtered map, zoomed in to 1°-by-1°

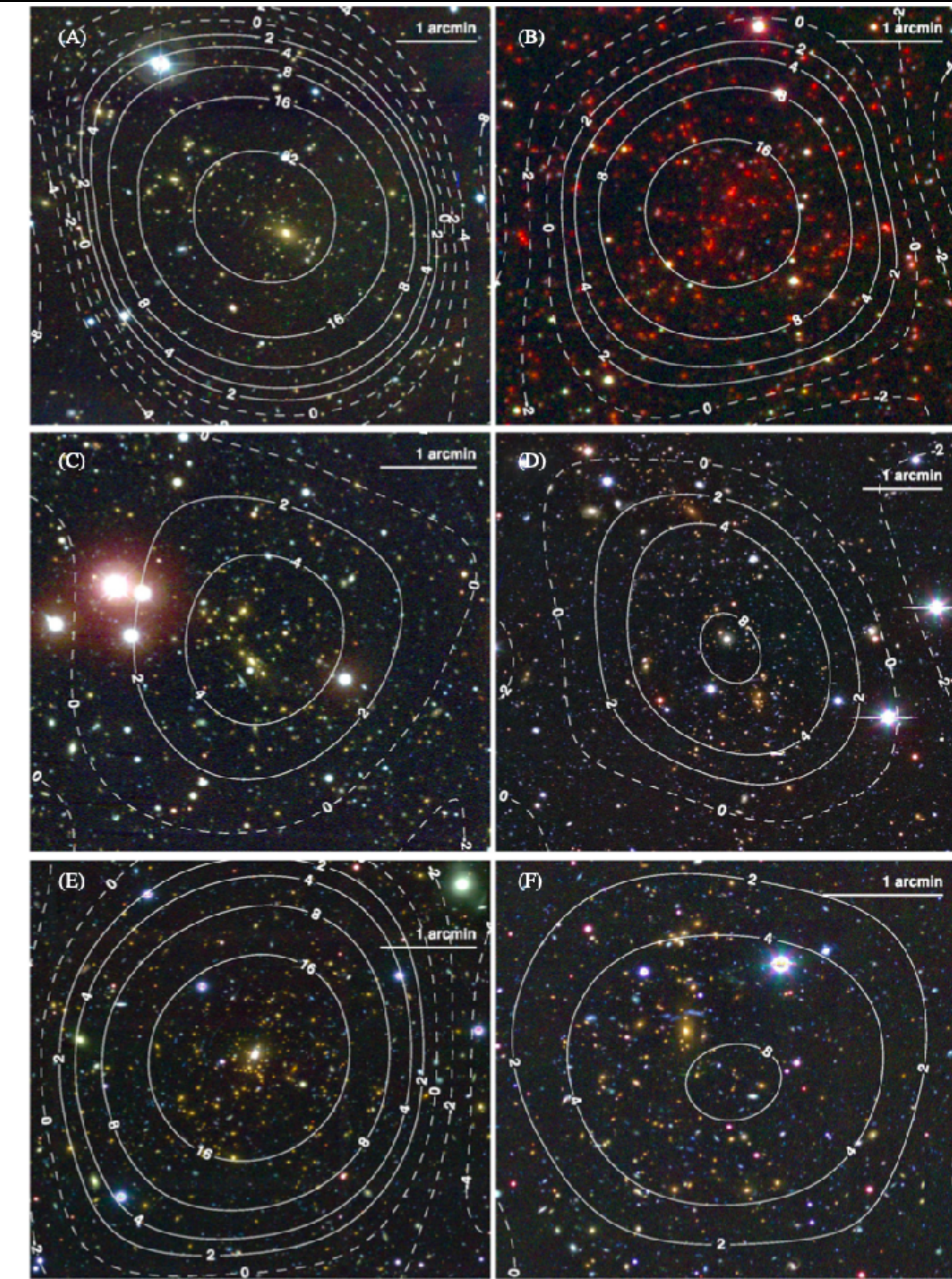


Figure 1. Visual representation of the SPT-SZ data and matched filtering process described in Sections 2 and 3. Panels (a) and (b) show 6° by 6° cutouts of 95 and 150 GHz maps from the RA21HDEC-60 field; the displayed temperature range is $\pm 300 \mu\text{K}$. These maps are made from data that have been only minimally filtered (scan-direction high-pass filter at $l \sim 50$) and show the main features of SPT-SZ survey data: large-scale primary CMB fluctuations, emissive point sources, and SZ decrements from galaxy clusters. Panel (c) shows the azimuthally averaged spatial-spectral filter optimized for detection of $\theta_c = 0.25$ clusters, with the red-dashed (blue-solid) curves showing the Fourier-domain coefficients for the 95 (150) GHz data. Panel (d) shows a zoomed-in view of the 1° -by- 1° area delineated by the dashed box in panel (b) after the spatial-spectral filter has been applied. This map is in units of signal-to-noise, and the displayed range is $-5 < \text{S/N} < 5$. Visible in this panel are the $\xi = 22.2, z = 1.132$ cluster SPT-CL J2106-5844 and the $\xi = 4.6$, optically unconfirmed candidate SPT-CL J2106-5820.

Figure 8. Sample of clusters from the 2500 deg^2 SPT-SZ cluster catalog. For each cluster we display an optical/NIR *rgb* image with the SZ detection contours over-plotted; see Section 6.4 for more details on particularly notable systems. (A) SPT-CL J2248-4431 (ACO S1063; $\xi = 42.4, z = 0.351$). This cluster is the most significant detection in the SPT sample (MPG/ESO WFI *IRV*-band image). (B) SPT-CL J2106-5844 ($\xi = 22.2, z = 1.132$)—also shown in SPT millimeter-wave data in Figure 1—is the most massive known cluster at $z > 1$. (*Spitzer*/IRAC $3.6 \mu\text{m}$, Magellan/FourStar *J*-band, Magellan/IMACS *i*-band image). (C) SPT-CL J0410-6343 ($\xi = 5.6, z = 0.52$) is a “typical” SPT cluster at approximately the median redshift and ξ of the confirmed cluster sample. (D) SPT-CL J0307-6224 ($\xi = 8.5, z = 0.581$) is undergoing a major merger. As SZ selection is not greatly influenced by mergers or complicated astrophysics at the cores of clusters (e.g., Motl et al. 2005; Fabjan et al. 2011), the SPT sample is representative of the entire population of massive clusters (Magellan/Megacam *gri*-band image). (E) SPT-CL J2344-4243 (the “Phoenix Cluster”; $\xi = 27.4, z = 0.596$) is the most X-ray luminous cluster known. We confirm this cluster as a strong lens using newly acquired Megacam imaging (Magellan/Megacam *gri*-band image). (F) SPT-CL J0307-5042 ($\xi = 8.4, z = 0.55$) is one of many strong-lensing clusters in the SPT sample (Magellan/Megacam *gri*-band image).

“空气一样的”暗物质

- Zwicky: 后发座星系团星系速度
- Rubin: 星系旋转速度
- 星系团: 气体 (微波SZ效应/X射线) , 水母星系, 强/弱引力透镜, 子弹星系团
- 星系团的产生: 局域非均匀宇宙 (晚期宇宙) ; 冷暗物质导致“自下而上”的层次结构形成
- 假如没有暗物质会发生什么
- 暗物质的微观测量

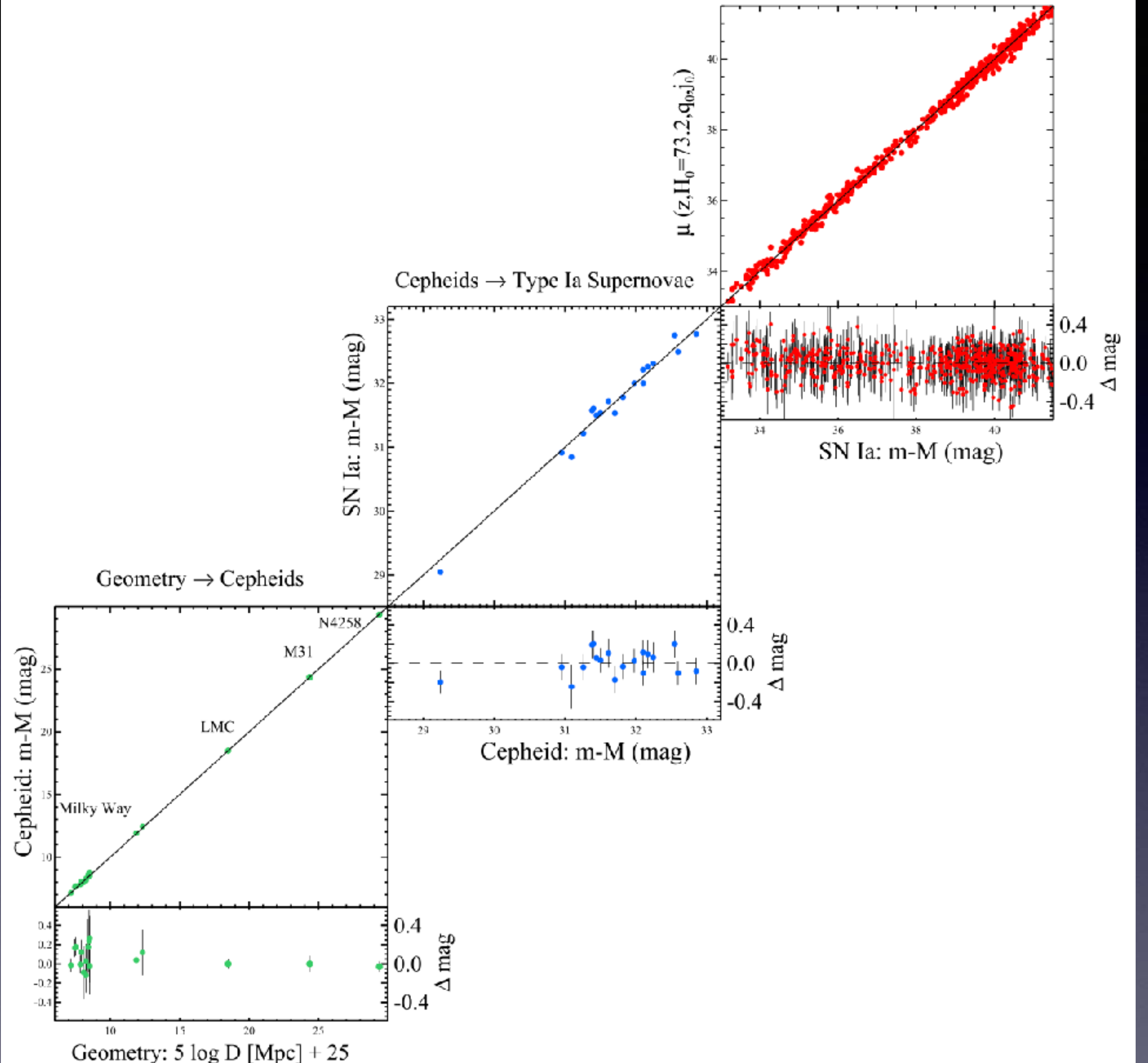


Figure 10. Complete distance ladder. The simultaneous agreement of pairs of geometric and Cepheid-based distances (lower left), Cepheid and SN Ia-based distances (middle panel) and SN and redshift-based distances provides the measurement of the Hubble constant. For each step, geometric or calibrated distances on the x-axis serve to calibrate a relative distance indicator on the y-axis through the determination of M or H_0 . Results shown are an approximation to the global fit as discussed in the text.

距离阶梯：几何法 → 造父变星 → Ia超新星 Riess+2016

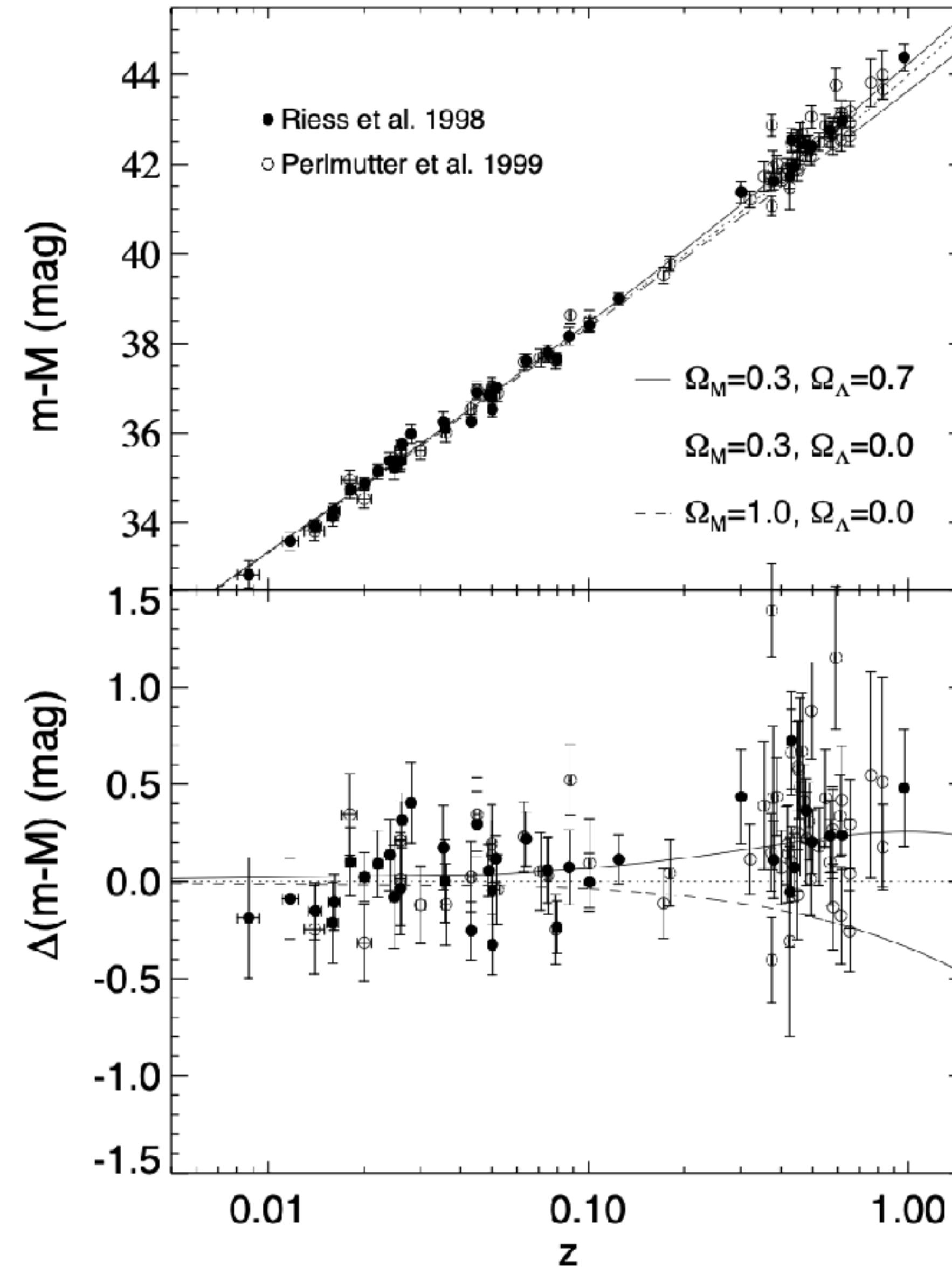


FIG. 1.—Hubble diagrams of SNe Ia from Perlmutter et al. (1999; SCP) and Riess et al. (1998; HZT). Overplotted are three cosmologies: “low” and “high” Ω_M with $\Omega_\Lambda = 0$ and the best fit for a flat cosmology, $\Omega_M = 0.3, \Omega_\Lambda = 0.7$. The bottom panel shows the difference between data and models from the $\Omega_M = 0.3, \Omega_\Lambda = 0$ prediction. The average difference between the data and the $\Omega_M = 0.3, \Omega_\Lambda = 0$ prediction is 0.28 mag.

宇宙加速膨胀
Riess 2000

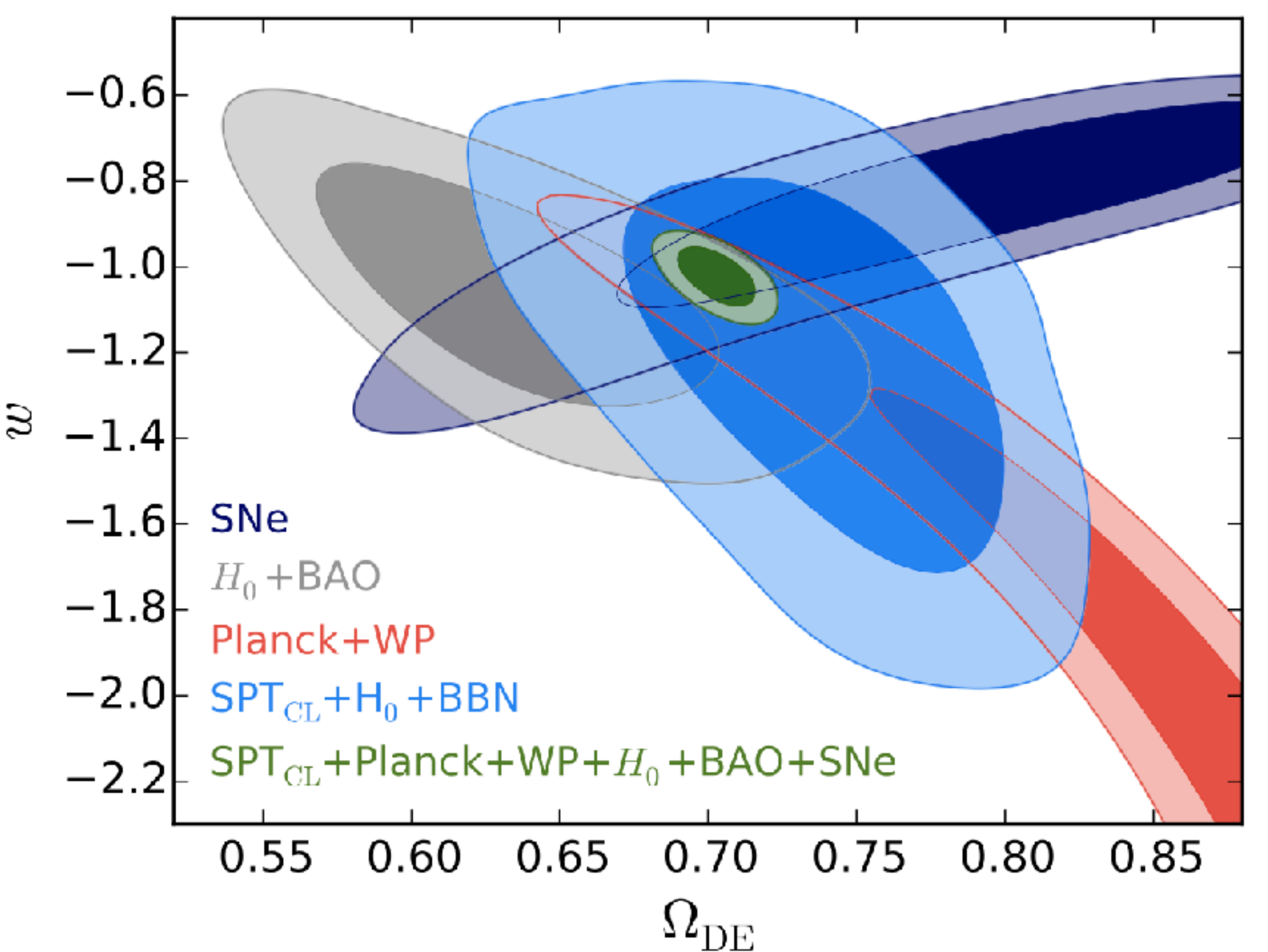


Figure 8. Comparison of different cosmological probes of dark energy. The contours show the simultaneous constraints on the present-day density of dark energy $\Omega_{\text{DE}} = 1 - \Omega_m$ and the dark energy equation of state parameter w . Using priors on H_0 and $\Omega_b h^2$, the SPT cluster data are able to simultaneously constrain the two parameters, and are in good agreement with the other probes. The other probes are sensitive to dark energy primarily through its effect on the geometry of the universe.

测量暗能量在宇宙中占比，压强密度比
de Haan+2016

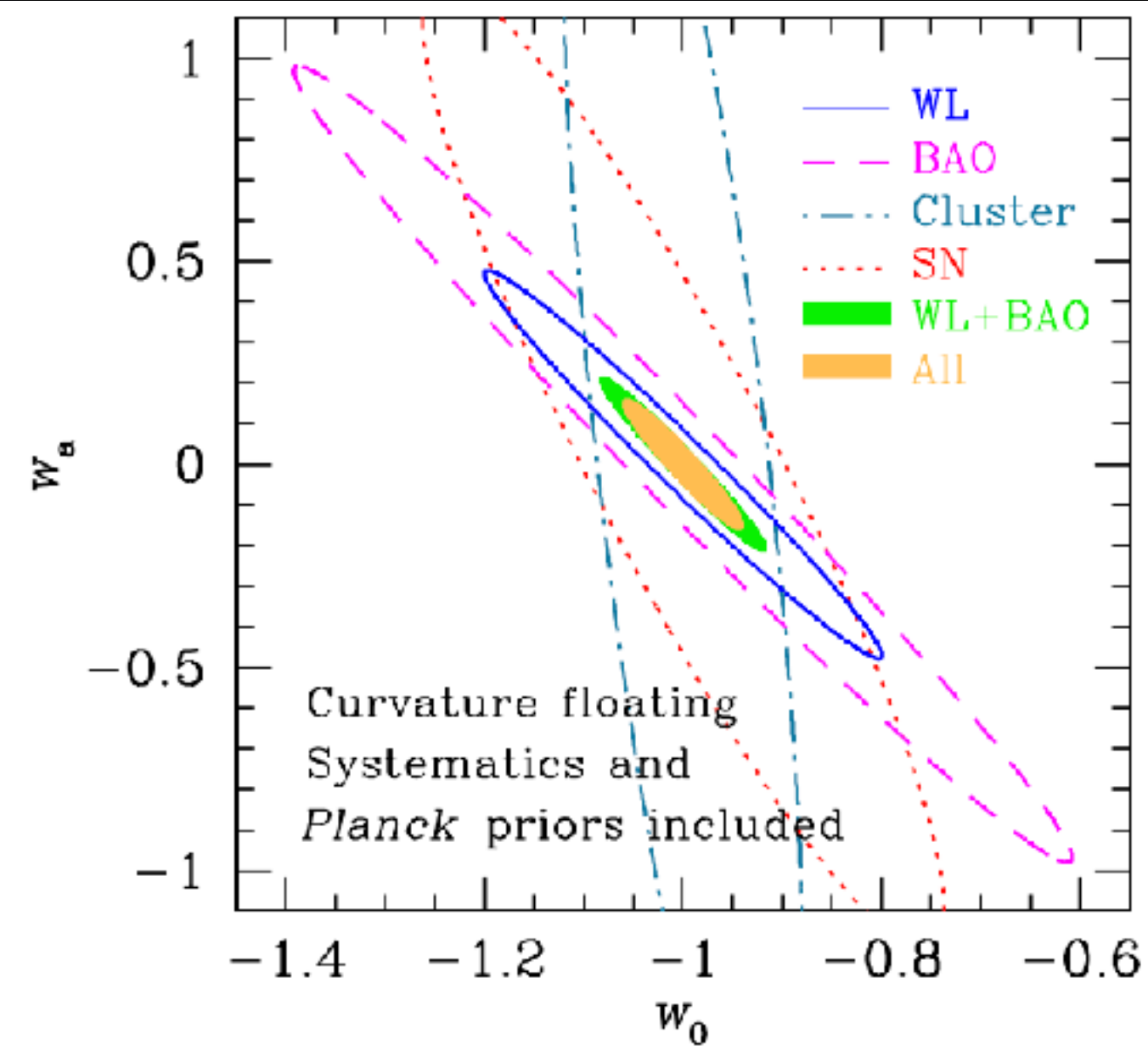


Figure 15.3: Joint w_0 - w_a constraints from LSST BAO (dashed line), cluster counting (dash-dotted line), supernovae (dotted line), WL (solid line), joint BAO and WL (green shaded area), and all combined (yellow shaded area). The BAO and WL results are based on galaxy-galaxy, galaxy-shear, and shear-shear power spectra only. Adding other probes such as strong lensing time delay (§ 12.4), ISW effect (§ 13.7), and higher-order galaxy and shear statistics (§ 13.5 and § 14.4) will further improve the constraints.

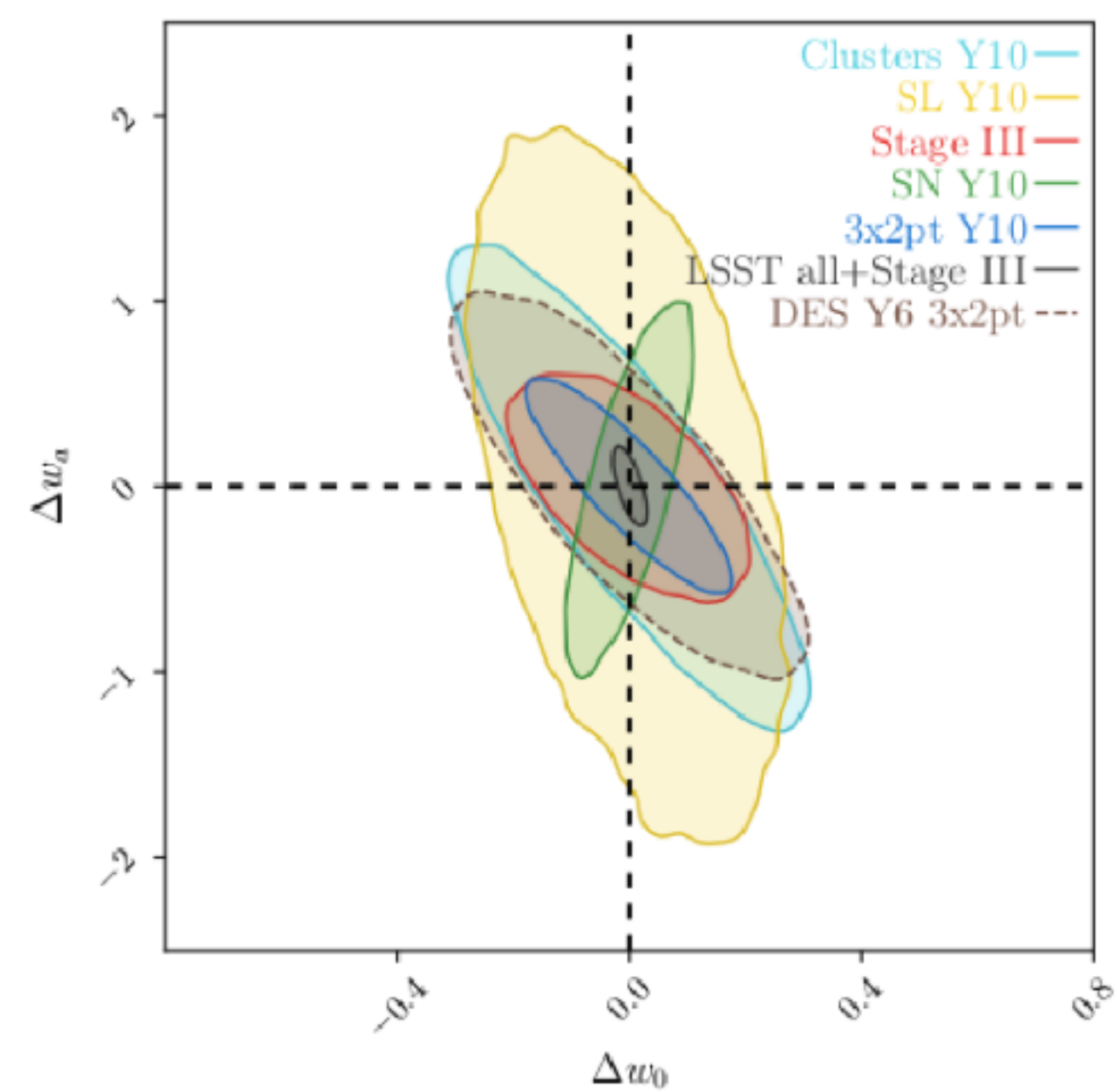


Figure 1: Expected 10 year constraints on time-varying dark energy combining all LSST cosmological probes, from the DESC SRD [2]. The contours labeled Stage III represent combined current constraints from the CMB, baryon acoustic oscillations, and supernovae. A possible realization of a DES Y6 3×2 pt analysis is included for comparison. LSST will clearly be a vast improvement over the current state of the art.

测量暗能量是否随时间变化
LSST Science Collaborations 2009;
Lochner+2018

“密度不随宇宙膨胀改变的”暗能量

- 宇宙膨胀速率， 加速膨胀
- Ia超新星， 标准烛光， 有多亮？ 太阳的几十亿倍， 接近星系核的亮度
- LambdaCDM， 宇宙的组成， 宇宙学常数 Lambda
- 临界质量， 平坦宇宙， 暴涨
- 重子声波震荡， 标准量天尺， 星系组成的“涟漪”
- 宇宙网， 星系团数量

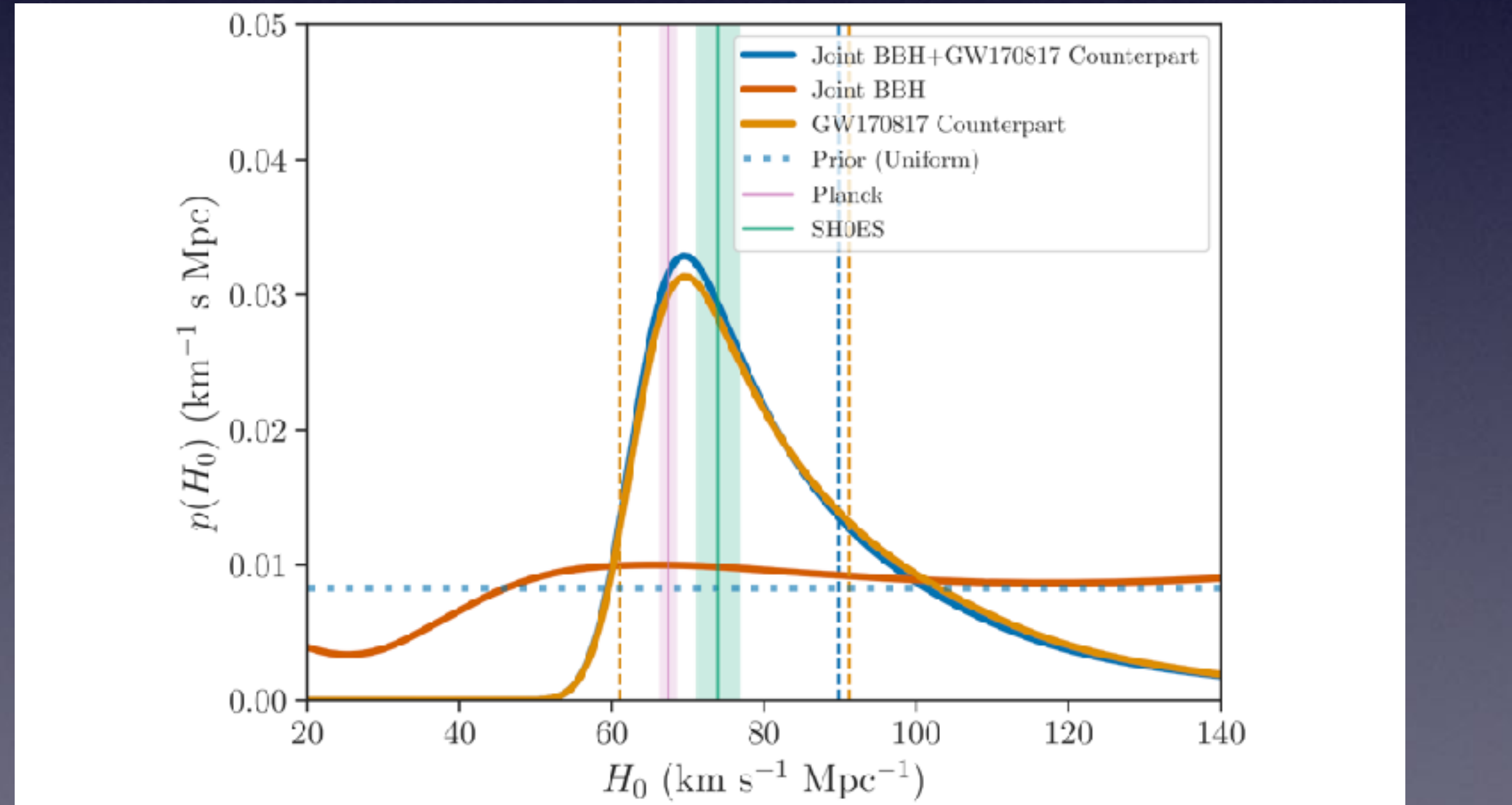
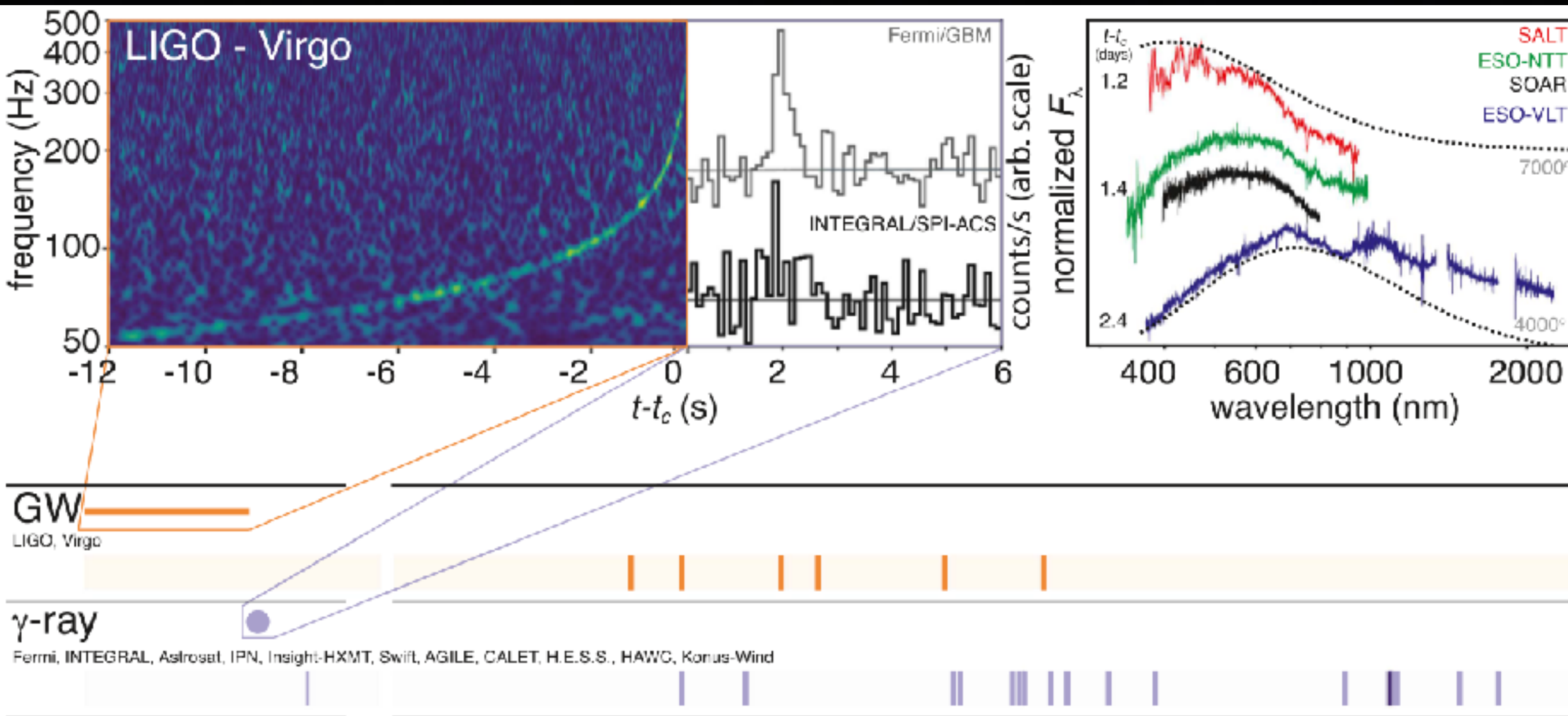
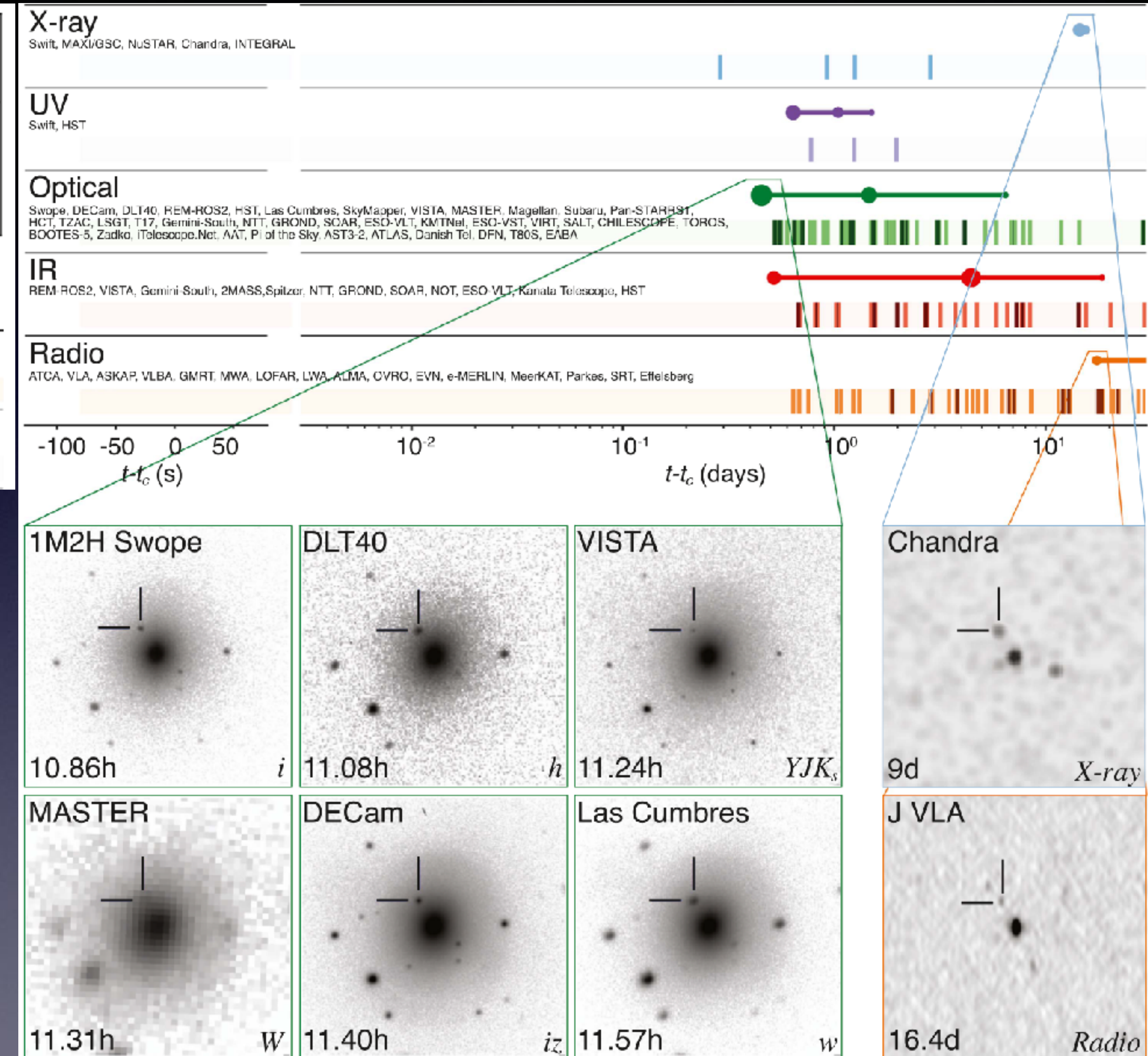


Figure 4. The GW measurement of H_0 (dark blue) from the detections in the first two observing runs of the Advanced LIGO and Virgo. The GW170817 estimate (orange) comes from the identification of its host galaxy NGC4993 (Abbott et al. 2017a). The additional contribution comes from BBHs in association with appropriate galaxy catalogs; for GW170814, we use the DES-Y1 galaxy catalog, while for the remaining five BBHs, GW150914, GW151226, GW170104, GW170608, and GW170809, we use the GLADE catalog. The 68% maximum a posteriori intervals are indicated with the vertical dashed lines. All results assume a prior on H_0 uniform in the interval $[20, 140] \text{ km s}^{-1} \text{ Mpc}^{-1}$ (dotted blue). We also show the estimates of H_0 from the CMB (Planck Collaboration et al. 2020) and supernova observations (SH0ES; Riess et al. 2019).



引力波, 千新星, 多信使天文 Abbott+2017

小结

- 日月星辰和古老的天文学
- 望远镜的发明改变了人们对宇宙的认识
- 科技的进步让人们能够看到宇宙的更多细节，建立起一套相对自洽的理论模型
- 人们还不清楚暗物质和暗能量的本质是什么
- 最后，希望大家保持对世界的好奇心